



# Persistent pollution episodes, transport pathways, and potential sources of air pollution during the heating season of 2016–2017 in Lanzhou, China

Yongtao Guo · Chunying Lin · Jiangping Li ·  
Lingbo Wei · Yuxia Ma · Qidong Yang ·  
Dandan Li · Hang Wang · Jiahui Shen

Received: 24 May 2021 / Accepted: 5 November 2021 / Published online: 30 November 2021  
© The Author(s), under exclusive licence to Springer Nature Switzerland AG 2021

**Abstract** As one of the most important industrial cities in Northwest China, Lanzhou currently suffers from serious air pollution. This study analyzed the formation mechanism and potential source areas of persistent air pollution in Lanzhou during the heating period from November 1, 2016 to March 31, 2017 based on the air pollutant concentrations and relevant meteorological data. Our findings indicate that particulate pollution was extremely severe during the study period. The daily  $PM_{2.5}$  and  $PM_{10}$  concentrations had significantly negative correlations with daily temperature, wind speed, maximum daily boundary layer height, while the daily  $PM_{2.5}$  and  $PM_{10}$  concentrations showed significantly positive correlations with daily relative humidity. Five persistent pollution episodes were identified and classified as either stagnant accumulation or explosive growth types according to the

mechanism of pollution formation and evolution. The  $PM_{2.5}$  and  $PM_{10}$  concentrations and  $PM_{2.5}/PM_{10}$  ratio followed a growing “saw-tooth cycle” pattern during the stagnant accumulation type event. Dust storms caused abrupt peaks in  $PM_{10}$  and a sharp decrease in the  $PM_{2.5}/PM_{10}$  ratio in explosive growth type events. The potential sources of  $PM_{10}$  were mainly distributed in the Kumtag Desert in Xinjiang Uygur Autonomous Region, the Qaidam Basin and Hehuang Valley in Qinghai Province, and the western and eastern Hexi Corridor in Gansu Province. The contributions to  $PM_{10}$  were more than  $120 \mu\text{g}/\text{m}^3$ . The important potential sources of  $PM_{2.5}$  were located in Hehuang Valley in Qinghai and Linxia Hui Autonomous Prefecture in Gansu; the concentrations of  $PM_{2.5}$  were more than  $60 \mu\text{g}/\text{m}^3$ .

Y. Guo (✉) · J. Li · L. Wei · Y. Ma · H. Wang · J. Shen  
College of Atmospheric Sciences, Lanzhou University,  
Lanzhou 730000, China  
e-mail: guoyt@lzu.edu.cn

C. Lin  
Qinghai Province Weather Modification Office,  
Xining 810001, China

Q. Yang  
Department of Atmosphere Science School of Earth  
Sciences, Yunnan University, Kunming 650500, China

D. Li  
Gansu Province Environmental Monitoring Center,  
Lanzhou 730020, China  
e-mail: ouyangtiandan@163.com

**Keywords** Air pollution · Persistent pollution ·  
Backward trajectory · Potential source contribution  
function · Concentration weighted trajectory

## Introduction

The rapid growth of industrialization and urbanization has led to severe and persistent air pollution in many cities of China in the last 30 years (Chen et al., 2017; Yu et al., 2020), which not only reduces atmospheric visibility (Liu et al., 2021), but also endangers human health (Ma et al., 2017). Thus, as one of the most serious environmental problems in urban areas, air

pollution has attracted attention from the government, the general public, and researchers. Generally, persistent air pollution is caused by meteorological conditions combined with local and regional sources of pollution (Deng et al., 2019; Gowan & Andrew, 2008).

Many studies have shown that stable synoptic circulation patterns along with other adverse meteorological conditions promote the accumulation of pollutants in the atmosphere, which leads to persistent air pollution (Annalisa et al., 2021; Liu et al., 2020). Liu et al. (2013) found that haze events in Beijing tended to occur more frequently under weak anticyclone synoptic conditions. Yang et al. (2015) reported that the primary factors driving haze formation in Beijing were a lack of atmospheric circulation, while a temperature inversion and high relative humidity (RH) accelerated the formation of regional haze. In addition, many studies have pointed out that regional transport significantly influences air pollution (Chifflet et al., 2018; Kozáková et al., 2019). Wang et al. (2015) provided a rough estimation that 35.5% of  $PM_{2.5}$  in Beijing was attributed to long-distance pollutant transportation using a potential source contribution function (PSCF) model. Zhao et al. (2016) also found that the Yangtze River Delta region was an important source region of humic-like substances in Shanghai by using a backward trajectory clustering and a concentration weighted trajectory (CWT) model.

Lanzhou is an industrial city in northwest China with petroleum refining, chemical engineering, and machinery manufacturing industries as its pillar industries. The city is surrounded by Gaolan Mountain in the south and Baita Mountain in the north (Fig. 1). Specific valley terrain can often make it difficult for pollutants to become diluted and diffused (Zhang & Hu, 1998; Zhang & Li, 2011). In the recent years, anthropogenic emissions caused

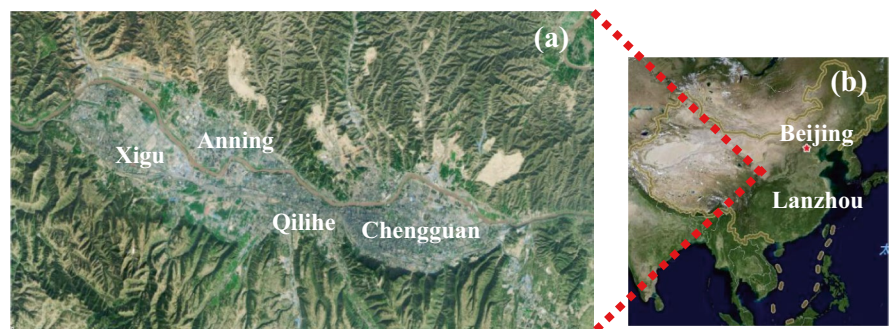
by the rapid development of Lanzhou have resulted in a serious increase in air pollution, especially in the heating season (Cheng et al., 2021; Guan et al., 2018). During this period, coal-fired emissions and the intensity of pollutant emissions increased significantly, resulting in frequent air pollution in Lanzhou (An et al., 2007; Chu et al., 2008a). Li (2018) found that in the non-heating season in Lanzhou, 20.9% of all days experienced significant air pollution from 2012 to 2016. Corresponding proportions of the heating season were 56.1%; the frequency of polluted days during the heating season was higher than during the non-heating season. From November 1, 2016 to March 31, 2017, several persistent air pollution events occurred, and one of them lasted from November 1 to 21, 2016. This persistent pollution in November 2016 was the worst air pollution event in recent years and had a wide impact and long duration. In order to alleviate air pollution, the local government urgently implemented an air pollution warning and launched traffic restriction measures based on license plate number for motor vehicles. The main goal of this study was to understand the formation mechanism involved in creating persistent pollution, explore potential sources of PM ( $PM_{2.5}$  and  $PM_{10}$ ), and quantify contributions of distant sources during the heating season from November 1, 2016 to March 31, 2017.

## Data and methodology

### Data

The concentration data for air pollutants ( $PM_{2.5}$ ,  $PM_{10}$ ,  $SO_2$ ,  $NO_2$ , and CO) in this study were derived from five state-owned automatic ambient

**Fig. 1** Location of Lanzhou within China: **a** aerial photo of Lanzhou showing four districts, Anning, Chengguan, Qilihe, and Xigu; **b** remote sensing photo showing the vicinity of Lanzhou and Beijing within China



air monitoring stations in Lanzhou. The ground and sounding meteorological data were obtained from Gansu Meteorological Administration in China. Dust storm data came from the monitoring station at Zhongchuan Airport, Lanzhou. The NCEP/NCAR reanalysis data were downloaded from the HYSPLIT (Hybrid Single-Particle Lagrangian Integrated Trajectory) website (available at <ftp://arlftp.arlhq.noaa.gov/pub/archives/gdas1/>).

*Methodology*

*Method for calculating the height of the maximum daily boundary layer* The boundary layer height is an important parameter used to represent how vertical diffusion conditions affect pollutants. It influences the concentrations of air pollutants (Shi et al., 2020). Variations in pollutant concentrations can be caused by changes in the boundary layer height over time (Zhu et al., 2019). Currently, the adiabatic curve method put forward by Holzworth (1964) is the main method used to determine the daily maximum boundary layer height ( $BLH_{max}$ ), which was applied in this study to estimate boundary layer height combined with the gradual approximation calculation method developed by Wang et al. (2000). The method was as follow by (1) calculation of the  $BLH_{max}$  using daily maximum temperature data based on the decline rate of the dry adiabatic temperature ( $\gamma_D=0.976/100$  m); it was calculated starting from ground level; the temperature was obtained every 50 m to an altitude of 3000 m; finally, a set of temperature values  $T_1, T_2, \dots, T_M$  was found at equal intervals of height; (2) on the actual temperature stratification curve (08 Radiosonde temperature profile data at Yuzhong meteorological station), a set of temperatures  $TT_1, TT_2, \dots, TT_M$  was also obtained by interpolation in the vertical direction with equal intervals of 50 m; (3) the temperature differences corresponding to T and TT were calculated at each height, and the temperature difference layer with the smallest absolute value was selected and identified as  $BLH_{max}$ .

*PSCF and CWT models* TrajStat software was used for cluster and potential source analysis. This software incorporates trajectory statistics and a geographical information system (Wang et al., 2009); it allows users to customize the trajectory and potential source maps,

which have been used in a number of prior publications (Huang et al., 2019; Bi et al., 2021). The 72-h backward air mass trajectories arriving at Lanzhou were calculated in this study by using a HYSPLIT model (Draxler & Hess, 1998). The NCEP/NCAR reanalysis dataset was used as meteorological data input to the model. The model was run at 00:00 UTC (08:00 local time (LT)) each day; the starting height was set at 500 m, which was chosen to diminish the effects of surface friction and to represent winds in the lower boundary layer (Hong et al., 2016). To compare the predominant transport pathways, backward trajectories were clustered into groups with similar transport pathways. The TrajStat software provides both angle and distance clustering methods. Here, we chose to use the angular distance, not the Euclidean distance, mainly because our interest was to use the trajectories to determine the direction from which the air masses that reached the site had been transported. The method used to calculate the mean angle between two trajectories was adapted from Sirois and Bottenheim (1995). A PSCF model was created to identify regional sources of  $PM_{2.5}$  and  $PM_{10}$  (Dimitriou & Kassomenos, 2018). The PSCF values for the grid cells were calculated by counting the trajectory segment endpoints that terminate within each cell. The zone of concern was divided into  $i \times j$  small equal grid cells. The grid covered a domain between 28–80° north latitude and 40–140° east longitude with a  $0.5^\circ \times 0.5^\circ$  resolution. The  $PSCF_{ij}$  was calculated using Eq. (1):

$$PSCF_{ij} = \frac{m_{ij}}{n_{ij}} \tag{1}$$

where  $n(i,j)$  is the number of endpoints that fall in the  $ij$ th cell and  $m(i,j)$  is the number of endpoints that fall in the  $ij$ th cell, corresponding to trajectories with pollutant concentrations higher than an arbitrary criterion value. Here, the criterion values were set at  $75 \mu\text{g}/\text{m}^3$  for  $PM_{2.5}$  and  $150 \mu\text{g}/\text{m}^3$  for  $PM_{10}$ . To remove the uncertainty in cells with small  $n_{ij}$  values, an empirical weight function  $W(n_{ij})$  as shown in Eq. (2) was multiplied with the PSCF value (Zhang et al., 2013):

$$w_{i,j} = \begin{cases} 1.00n_{i,j} > 2.0n_{avg} \\ 0.70n_{avg} < n_{i,j} \leq 2.0n_{avg} \\ 0.420.5n_{avg} < n_{i,j} \leq n_{avg} \\ 0.170 < n_{i,j} \leq 0.5n_{avg} \end{cases} \tag{2}$$

A PSCF model reflects only the proportion of pollution trajectories in a grid, and cannot reflect the trajectory of pollution levels. To compensate for this limitation, the CWT method developed by Hsu et al. (2003) was used to calculate the weighted trajectory concentration. The CWT value for the  $ij$ th cell was calculated by the Eq. (3):

$$C_{i,j} = \frac{1}{\sum_{l=1}^M \tau_{ijl}} \sum_{l=1}^M C_l \tau_{ijl} \quad (3)$$

where  $C_{i,j}$  is the mean weighted concentration in the cell ( $i,j$ ),  $l$  is the index of the trajectory,  $M$  is the total number of trajectories,  $C_l$  is the observed concentration related to the arrival trajectory  $l$ , and  $\tau_{ijl}$  is the time spent in the cell ( $i,j$ ) by trajectory  $l$ . The arbitrary weighting function described above was also used in the CWT analyses to reduce the effect of the small values of  $n_{ij}$ .

## Results

### General meteorological conditions and air pollution characteristics

In this study, November 1, 2016 to March 31, 2017 was defined as the heating season. The daily mean concentrations of particulates ( $PM_{2.5}$ ,  $PM_{10}$ ) and gaseous pollutants ( $SO_2$ ,  $NO_2$ , and CO) during the heating period are shown in Table 1. Except for CO,  $PM_{10}$  exhibited the highest concentration among all of the air pollutants, with a daily mean concentration at  $177 \pm 142 \mu\text{g}/\text{m}^3$ , followed by  $PM_{2.5}$  ( $70 \pm 32 \mu\text{g}/\text{m}^3$ ). About 53% of the daily  $PM_{10}$  concentration exceeded the Chinese Ambient Air Quality Grade II standard of  $150 \mu\text{g m}^{-3}$  (GB3095-2012), while 37% of the daily  $PM_{2.5}$  concentration surpassed the Grade II standard ( $75 \mu\text{g m}^{-3}$ ). The daily mean concentrations of  $SO_2$ ,  $NO_2$ , and CO were  $29 \pm 12 \mu\text{g}/\text{m}^3$ ,  $64 \pm 25 \mu\text{g}/\text{m}^3$ , and  $1.6 \pm 0.71 \text{ mg}/\text{m}^3$ , respectively; the daily  $NO_2$  concentration exceeded the Grade II standard ( $80 \mu\text{g m}^{-3}$ ) 28% of the time; meanwhile, the daily  $SO_2$  and CO concentrations never exceeded the Grade II standard ( $150 \mu\text{g m}^{-3}$  for  $SO_2$ ,  $4 \text{ mg}/\text{m}^3$  for CO). This indicates that particulate pollution was extremely severe during the heating season while current situations of gaseous pollution were generally much better. Thus, PM

**Table 1** Descriptive statistics of the air pollutants during the heating season between November 1, 2016 and March 31, 2017 in Lanzhou

	$PM_{2.5}$	$PM_{10}$	$SO_2$	$NO_2$	CO
Mean	70	176	29	64	1.6
S.D	32	142	12	25	0.7
Min	25	47	8	19	0.6
Max	213	1398	57	122	3.5
Exceeding-standard rate	37%	53%	0%	28%	0%

Air pollutants were measured as  $\mu\text{g}/\text{m}^3$ , with the exception of CO (using  $\text{mg}/\text{m}^3$ )

( $PM_{2.5}$  and  $PM_{10}$ ) levels are discussed in the next section in detail.

Table 2 shows the mean temperature, wind speed, RH, and  $BLH_{\text{max}}$  were  $3.8 \pm 5.5 \text{ }^\circ\text{C}$ ,  $1.1 \pm 0.3 \text{ m/s}$ ,  $46 \pm 13.6\%$ , and  $871 \pm 493.8 \text{ m}$ , respectively. The mean value of temperature, wind speed, and  $BLH_{\text{max}}$  above the Grade II standard were lower than the mean value of temperature wind speed and  $BLH_{\text{max}}$  below the Grade II standard; however, the mean value of RH above the Grade II standard was higher than the mean value of RH below the Grade II standard. The linear relationship between the meteorological factors and PM was quantified using Spearman correlation tests (Table 3); the correlation coefficients between all of the meteorological factors except RH and PM were significantly negative, which varies between 0.46 and 0.65; the RH showed a significantly positive correlation with both  $PM_{10}$  ( $r=0.41$ ) and  $PM_{2.5}$  ( $r=0.56$ ) in this study.

### The formation and maintenance mechanism of persistent pollution

#### Classification of persistent pollution

The concept of a persistent pollution episode refers to a temporal process when pollutants accumulate high in the atmosphere where they remain for some time before cleaner air conditions return. The pollutant levels and durations of such episodes differed in several studies (Sun et al., 2019; Tan et al., 2018). In the present study, an Air Quality Index (as defined by China's Ministry of Environmental Protection) above 100 for five or more consecutive days was defined as a persistent pollution episode. Figure 2 shows that five

**Table 2** Statistical characteristics of meteorological parameters in the heating season, below and above the Grade II standard levels during the heating season from November 1, 2016 to March 31, 2017 in Lanzhou

	T (°C)	Wind (m/s)	RH (%)	BLH <sub>max</sub> (m)
The heating season	3.8 ± 5.5	1.1 ± 0.3	46 ± 13.6	871 ± 493.8
PM <sub>10</sub>				
Below the Grade II standard	1.90 ± 3.8	1.70 ± 0.2	45.43 ± 12.5	1153 ± 389.7
Above the Grade II standard	1.68 ± 3.2	0.98 ± 0.3	47.56 ± 13.1	848 ± 305.3
PM <sub>2.5</sub>				
Below the Grade II standard	2.11 ± 3.8	1.18 ± 0.3	44.06 ± 12.8	1151 ± 368.9
Above the Grade II standard	1.17 ± 2.7	0.87 ± 0.2	50.89 ± 11.5	728 ± 219.3

persistent pollution episodes were observed according to this definition; Table 3 provides the dates for these episodes. Among them, the second persistent pollution episode had the most intense and sustained period of pollution which lasted for 21 days from November 1 to 21, 2016. A prominent feature of this episode was that abrupt peaks of PM<sub>10</sub> were observed without a notable increase in gaseous pollutants. For example, the PM<sub>10</sub> concentration increased to 946 µg/m<sup>3</sup> on November 10, 2016, which was the maximum daily PM<sub>10</sub> concentration. This was mainly caused by a dust storm.

The mean air pollutant concentrations and meteorological parameters in five persistent pollution episodes are summarized in Table 4. These episodes could be categorized into stagnant accumulation and explosive growth types based on their pollution and meteorological characteristics. The stagnant accumulation type was characterized by high PM<sub>2.5</sub> and PM<sub>10</sub> concentrations and a high PM<sub>2.5</sub>/PM<sub>10</sub> ratio, which was mainly associated with persistently stable meteorological conditions, such as low temperature and calm wind. The second persistent pollution episode belongs to this type. The explosive growth type was caused by secondary particles in periods with stable meteorological conditions and a massive amount primary particles brought into the study area by dust storms. This type could be divided into two stages:

**Table 3** Spearman correlation coefficients between meteorological factors and particulate matter (PM<sub>10</sub>, PM<sub>2.5</sub>) during the heating season from November 1, 2016 to March 31, 2017 in Lanzhou

	T	Wind	RH	BLH <sub>max</sub>
PM <sub>10</sub>	0.48*	0.51*	0.41*	0.46*
PM <sub>2.5</sub>	0.56*	0.72*	0.56*	0.65*

\* This indicates  $p < 0.01$

stagnant accumulation (stage 1) and explosive growth (stage 2). Taking Ep1 as an example, the mean temperature and wind speed in stage 1 were low, which were  $6.3 \pm 1.4$  °C and  $0.7 \pm 0.1$  m/s, respectively; the mean relative humidity in stage 1 was relatively high at  $65 \pm 9\%$ , indicated that the atmosphere was stagnant allowing pollutants to easily accumulate. The PM<sub>2.5</sub> and PM<sub>10</sub> concentrations were  $106 \pm 6$  µg/m<sup>3</sup> and  $224 \pm 19$  µg/m<sup>3</sup>, respectively, and the PM<sub>2.5</sub>/PM<sub>10</sub> ratio was relatively high at  $0.48 \pm 0.1$ . Also, the mean temperature and relative humidity in stage 2 were reduced compared with the previous stage at  $5.2 \pm 0.9$  °C and  $47 \pm 7\%$ , respectively; this indicated the arrival of cold air. The mean PM<sub>10</sub> concentration suddenly increased in stage 2 because of dust particulate transportation accompanied by cold air, which was  $503 \pm 273$  µg/m<sup>3</sup>. Meanwhile, the PM<sub>2.5</sub>/PM<sub>10</sub> ratio decreased significantly to  $0.27 \pm 0.1$ .

Growth pattern of PM<sub>10</sub> and PM<sub>2.5</sub> during persistent pollution episodes

Figure 3 shows the variations of the PM<sub>2.5</sub> and PM<sub>10</sub> concentrations and the PM<sub>2.5</sub>/PM<sub>10</sub> ratio in a high time resolution (1 h) during two selected persistent periods of pollution (Ep1, November 1 to 21, 2016; Ep2, November 31 to December 14, 2016). The others belonged to the explosive growth type and the patterns were similar to that of Ep1, so they were ignored. The PM<sub>2.5</sub> and PM<sub>10</sub> concentrations had different growth characteristics in the two types (Fig. 3). They showed an asymmetric “saw-tooth cycle” growth in the stagnant accumulation type (Ep2). First, the PM<sub>2.5</sub> and PM<sub>10</sub> concentrations and PM<sub>2.5</sub>/PM<sub>10</sub> ratio (red line in Fig. 3b) rose gradually, and maintained for some time. This was interrupted by an incomplete removal process. This was followed by a new cycle where



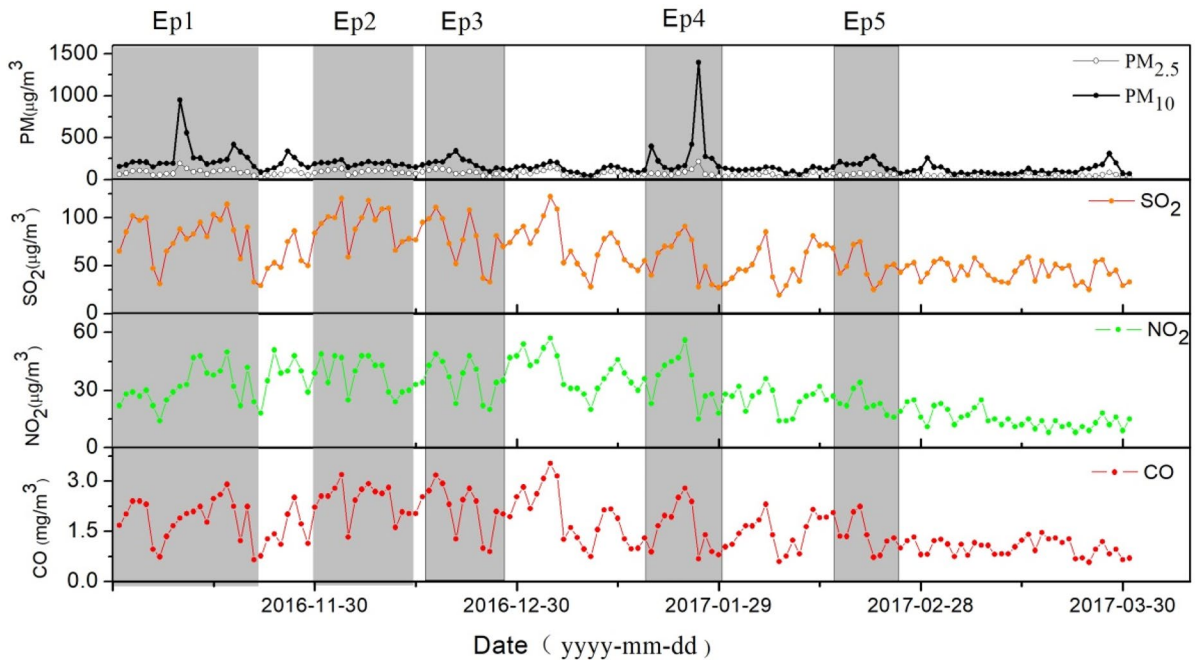


**Fig. 2** The variations of the concentrations of  $PM_{2.5}$ ,  $PM_{10}$ ,  $SO_2$ ,  $NO_2$ , and  $CO$  during the heating season from November 1, 2016 to March 31, 2017 in Lanzhou. Dates for five typical

persistent pollution periods (Ep1 to Ep5) are shown; Table 4 provides the dates for these periods

the process was not ended until the weather conditions improved. Figure 3a shows that the explosive growth type (Ep1) was divided into two evolution stages; this was also an asymmetric “saw-tooth cycle” growth in stage 1. At the same time,  $PM_{10}$

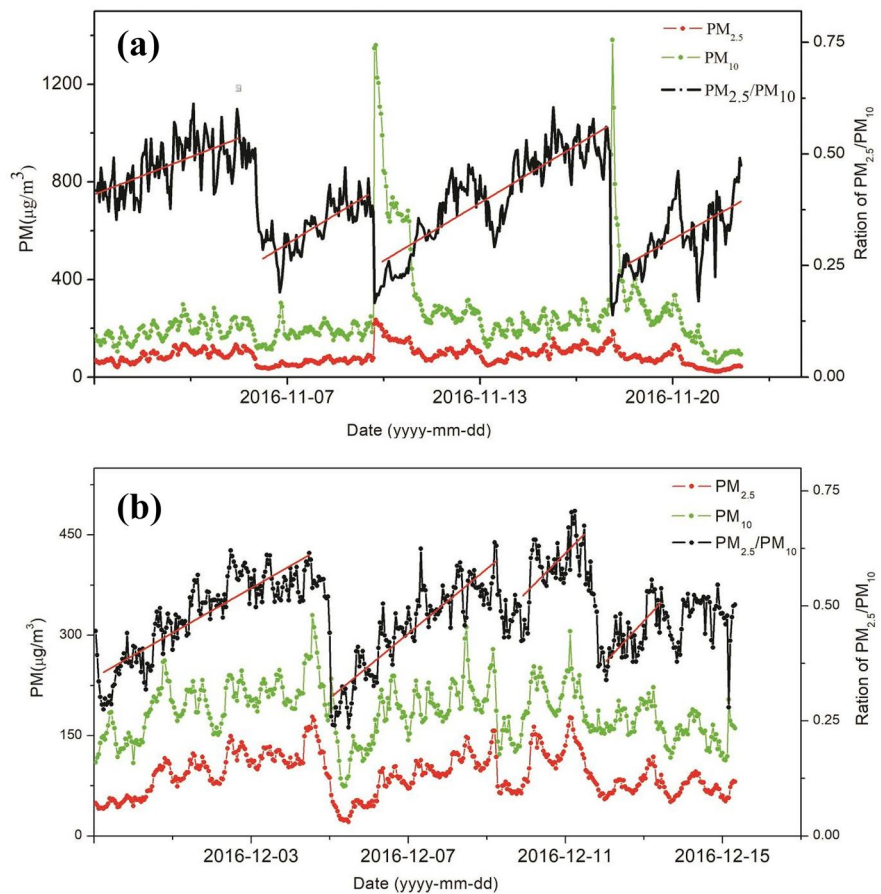
had an explosive growth accompanied by  $PM_{2.5}/PM_{10}$  ratio falling sharply in stage 2. Finally, as each dust storm weakened, the  $PM_{2.5}$  and  $PM_{10}$  concentrations decreased slowly, while the  $PM_{2.5}/PM_{10}$  ratio also gradually increased.

**Table 4** Characteristics of  $PM_{2.5}$  and  $PM_{10}$  concentrations and meteorological factors in five persistent pollution episodes (Ep1 to Ep5) during the heating season from November 1, 2016 to March 31, 2017 in Lanzhou

Ep	Start and end time	Stage	$PM_{2.5}$ ( $\mu\text{g}/\text{m}^3$ )	$PM_{10}$ ( $\mu\text{g}/\text{m}^3$ )	$PM_{2.5}/PM_{10}$	T ( $^{\circ}\text{C}$ )	RH (%)	Wind (m/s)
Ep1	2016/11/1–11/21	1	$106 \pm 6$	$224 \pm 19$	$0.48 \pm 0.1$	$6.3 \pm 1.4$	$65 \pm 9$	$0.7 \pm 0.1$
		2	$124 \pm 44$	$503 \pm 273$	$0.27 \pm 0.1$	$5.2 \pm 0.9$	$47 \pm 7$	$0.9 \pm 0.1$
Ep2	2016/11/30–12/14	1	$115 \pm 12$	$208 \pm 16$	$0.55 \pm 0.1$	$1.0 \pm 1.1$	$55 \pm 5$	$0.8 \pm 0.1$
Ep3	2016/12/16–12/24	1	$122 \pm 10$	$205 \pm 10$	$0.59 \pm 0.1$	$-1.1 \pm 1.0$	$56 \pm 1$	$0.8 \pm 0.1$
		2	$87 \pm 19$	$271 \pm 53$	$0.33 \pm 0.1$	$-0.5 \pm 1.2$	$50 \pm 4$	$1.0 \pm 0.1$
Ep4	2017/1/23–1/29	1	$85 \pm 10$	$157 \pm 60$	$0.54 \pm 0.0$	$0.7 \pm 1.4$	$30 \pm 3$	$1.0 \pm 0.2$
		2	$98 \pm 72$	$499 \pm 511$	$0.22 \pm 0.1$	$1.1 \pm 1.0$	$30 \pm 6$	$1.2 \pm 0.4$
Ep5	2017/2/12–2/22	1	$70 \pm 11$	$171 \pm 22$	$0.59 \pm 0.0$	$5.6 \pm 0.9$	$30 \pm 6$	$1.1 \pm 0.2$
		2	$61 \pm 9$	$236 \pm 48$	$0.26 \pm 0.1$	$2.2 \pm 3.7$	$46 \pm 13$	$1.5 \pm 0.2$

Stages 1 and 2 are the stagnant accumulation and explosive growth stages, respectively  
*T* temperature, *RH* relative humidity

**Fig. 3** The high time resolution variation of particulate matter ( $PM_{10}$ ,  $PM_{2.5}$ ) and its ratio during two persistent pollution emission periods, Ep1 (November 1 to 21, 2016) and Ep2 (November 31 to December 14, 2016)



Synoptic circulation and characteristics of meteorological factors of persistent pollution

An analysis of the 500 hPa synoptic circulation over Lanzhou during the five persistent pollution episodes found that the circulation was primarily controlled by the zonal circulation (such as straight westerly airflow and weak frontal systems). The prevailing airflow was from the west and northwest; when the synoptic circulation shifted, Lanzhou was located at the front of a cyclone system or short-wave trough except for Ep2, indicating that cold air advection transited the region. Examples of the synoptic circulation for selected persistent pollution episodes are provided in Fig. 4. During Ep2, a high-pressure ridge covered the study area on December 30 when the atmosphere was stable (Fig. 4c, d). As the synoptic circulation shifted on November 12, Lanzhou was located behind the trough and in front of the ridge, indicating the atmosphere still remained stable. The synoptic circulation in stage

1 of Ep1 (Fig. 4a) was very similar to that in Ep2 on December 30. One notable difference was that a cyclone system developed in stage 2 of Ep1 (Fig. 4b) and was located to the west of Mongolia; Lanzhou lay on its southeastern edge, and experienced the arrival of cold air (Fig. 5).

Variable characteristics of surface meteorological factors and the boundary layer in persistent pollution

Figure 6 shows the daily variations in meteorological conditions for two selected persistent pollution episodes, Ep1 and Ep2. The temperature and wind speed were lower than 2.5 °C and 1.1 m/s during Ep2, respectively (Fig. 6c, d). The  $BLH_{max}$  was very low and varied between 286 and 975 m. The variations in meteorological conditions during Ep1 could be roughly divided into two stages (Fig. 6a, b). The meteorological factors during stage 1 (November 1 to 4, 2016) involved low temperature, wind speed, and

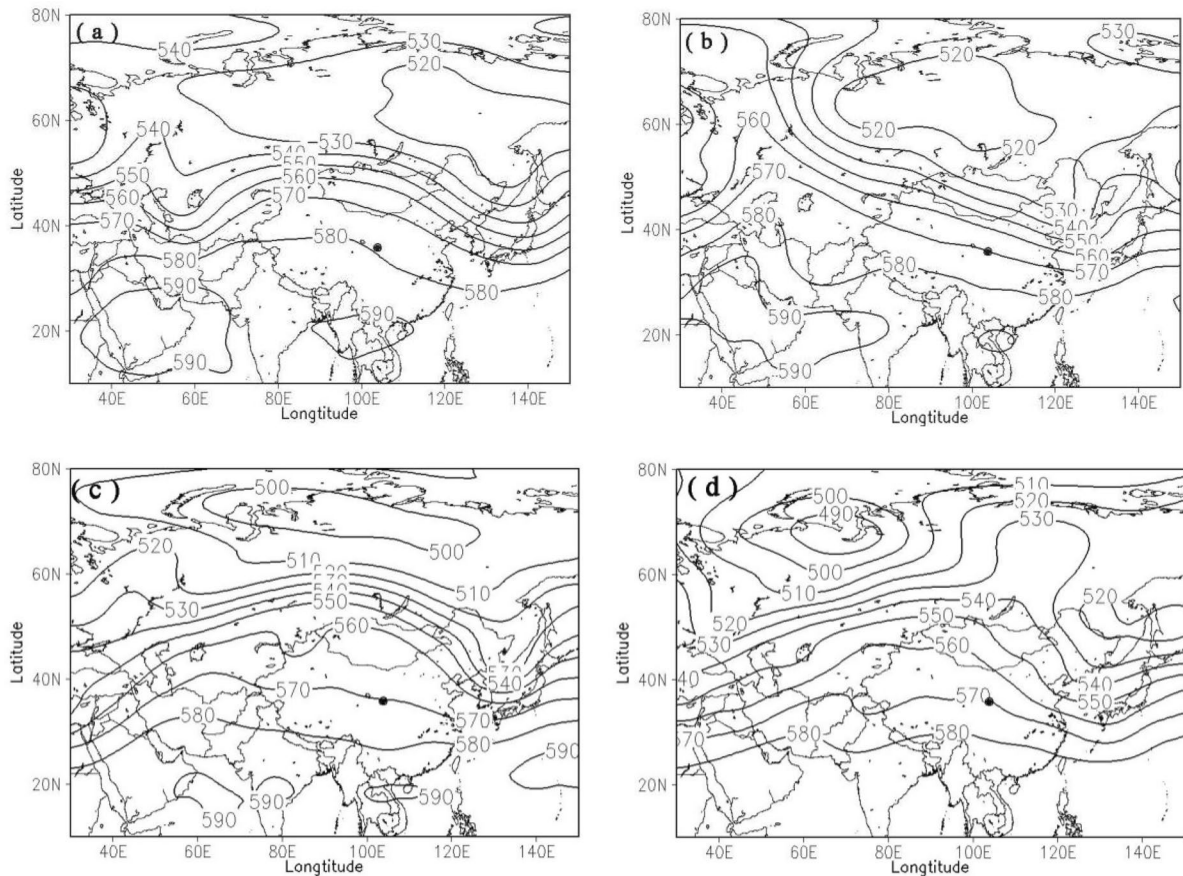


**Fig. 4** Synoptic maps on two persistent pollution periods: **a** 18:00 local time (LT), November 2, 2016; **b** 18:00 LT, November 10, 2016 for Ep1 and **c** 18:00 LT, November 30, 2016; **d** 06:00 LT, December 12, 2016) for Ep2 and for 500 hPa

$BLH_{max}$ . Compared to stage 1, the most significant difference was the lower temperatures and RH, and higher  $BLH_{max}$  in stage 2 (November. 5 to 19, 2016).

#### Statistical analysis of potential source areas

##### Cluster analysis

In order to explore the influence of air masses on  $PM_{2.5}$  and  $PM_{10}$  in Lanzhou, TrajStat software was used to simulate and cluster the 72-h backward trajectories during the study period. All of trajectories were grouped into five clusters, which are described in Fig. 7b. Cluster 1 from the west had the highest frequency (64.6%) of the five clusters, followed by cluster 4 from the southwest with 11.6%, while cluster 2 contributed the least (4.6%) to the total

trajectories. Table 5 shows corresponding daily mean  $PM_{2.5}$  and  $PM_{10}$  concentration in five clusters in this study. The highest  $PM_{10}$  concentrations were related to clusters 1 and 5, at  $205 \pm 176 \mu\text{g}/\text{m}^3$  and  $148 \pm 48 \mu\text{g}/\text{m}^3$ , respectively (Table 5). The highest  $PM_{2.5}$  concentrations were observed in clusters 1 and 4 at  $78 \pm 33 \mu\text{g}/\text{m}^3$  and  $73 \pm 27 \mu\text{g}/\text{m}^3$ , respectively (Table 5). The lowest  $PM_{10}$  and  $PM_{2.5}$  concentrations, which were  $105 \pm 27 \mu\text{g}/\text{m}^3$  and  $41 \pm 33 \mu\text{g}/\text{m}^3$ , respectively, were found in cluster 2 (Table 5).

##### Weighted PSCF and weighted CWT

The weighted PSCF (WPSCF) maps of  $PM_{10}$  and  $PM_{2.5}$  in Lanzhou during the study period is shown in Fig. 8 The higher the value of WPSCF, the greater



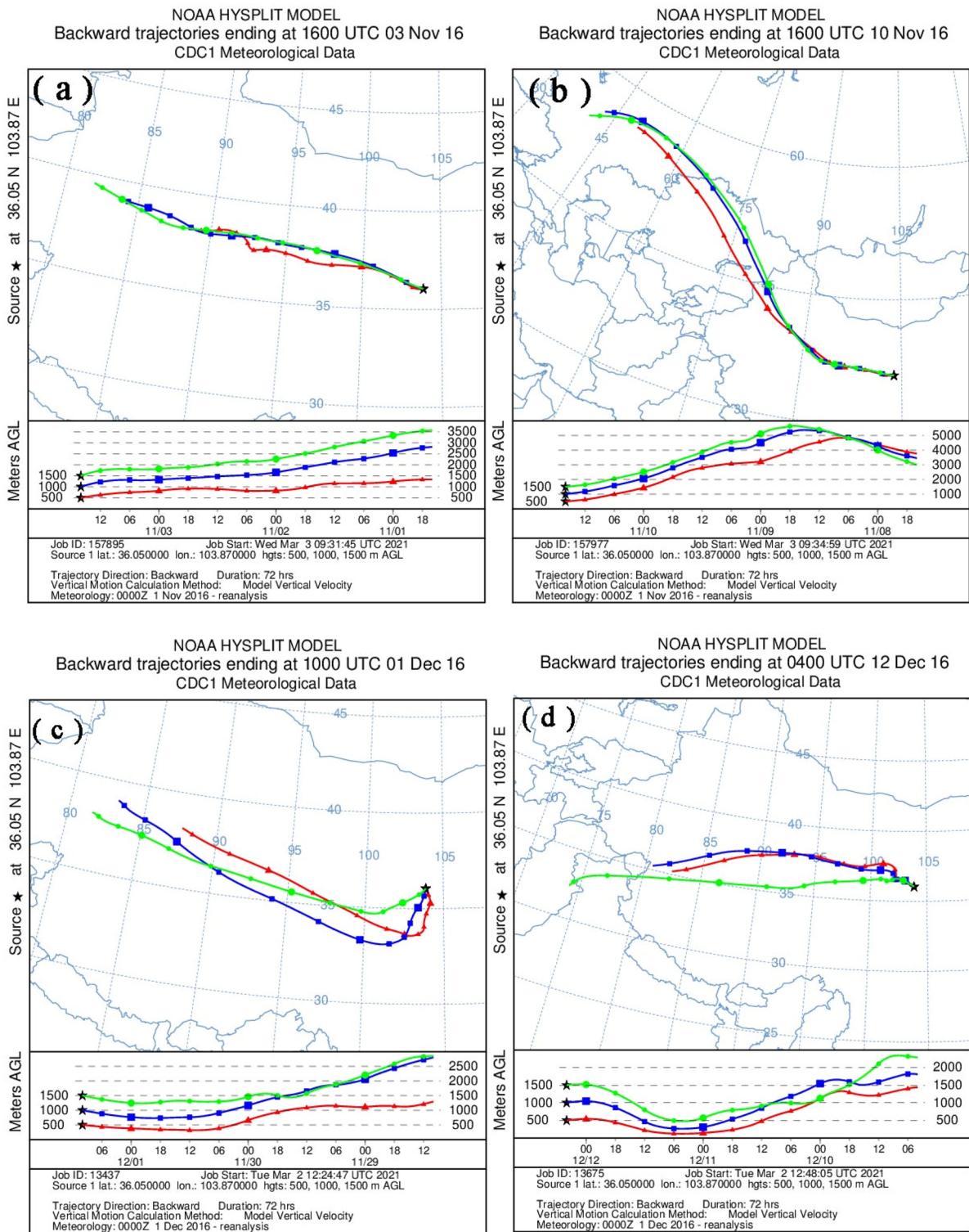


**Fig. 5** Modeling of 72 h-backward trajectories during two persistent pollution periods **a, b** Ep1 (November 1 to 21, 2016) and **c, d** Ep2 (November 31 to December 14, 2016) using the US National Oceanic and Atmospheric Administration Hysplit Model

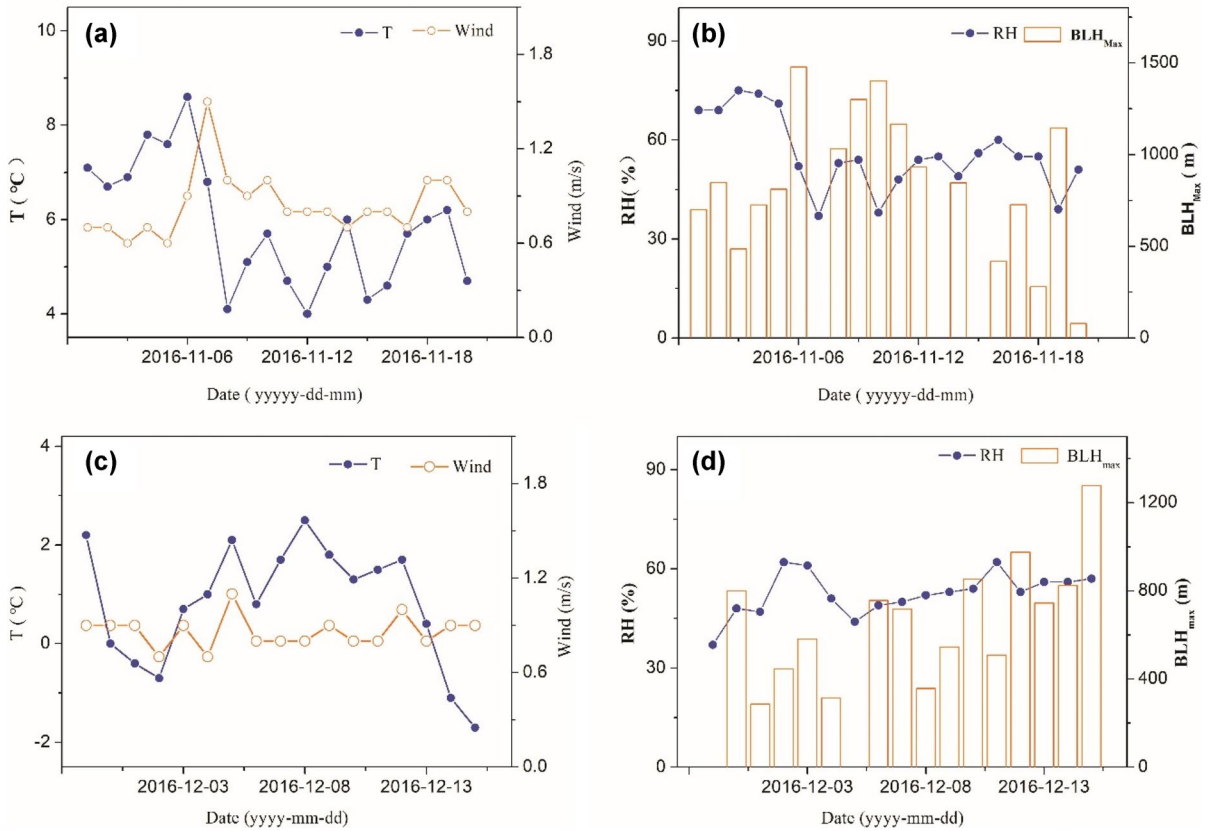


**Fig. 6** Daily variations in **a, c** temperature, **b, d** Wind and RH, and BLH<sub>max</sub> during two persistent pollution emission periods, Ep1 (November 1 to 21, 2016) and Ep2 (November 31 to December 14, 2016)

the impact on PM<sub>10</sub> and PM<sub>2.5</sub>. Higher WPSCF values of PM<sub>10</sub> were observed in the Kumtag Desert in the western Xinjiang, the Qaidam Basin and the

Hehuang Valley of Qinghai, as well as in the western and eastern Hexi Corridor in Gansu (Fig. 8a). These values were mostly between 0.4 and 0.6, although

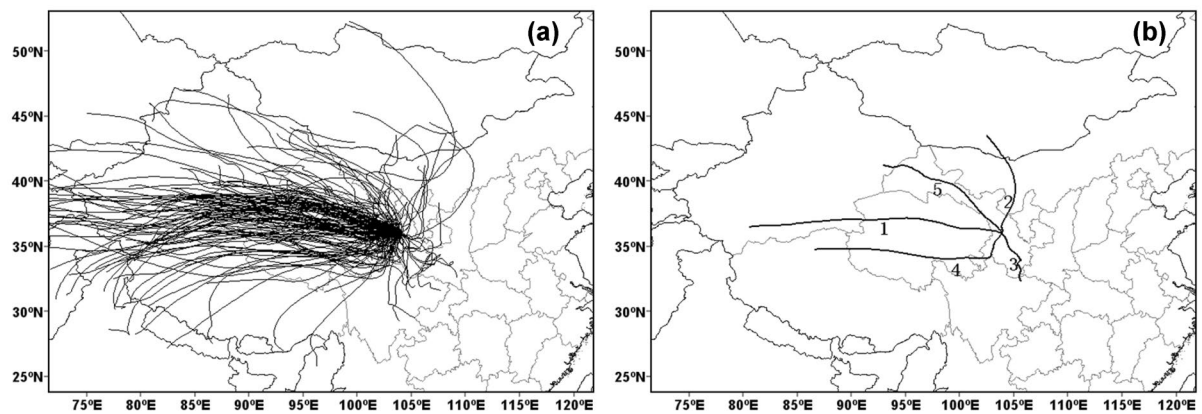


**Fig. 7** TrajStat software used to simulate and cluster **a** the 72-h backward trajectory distribution and **b** mean backward trajectory clusters during the heating season from November 1, 2016 to March 31, 2017 in Lanzhou

**Table 5** Summary statistics of PM<sub>2.5</sub> and PM<sub>10</sub> concentrations in Lanzhou associated with clusters 1 to 5 during the heating season from November 1, 2016 to March 31, 2017 in Lanzhou

Cluster group	Number	Percentage (%)	PM <sub>10</sub> (µg/m <sup>3</sup> )	PM <sub>2.5</sub> (µg/m <sup>3</sup> )
1	95	64.6	205 ± 176	78 ± 33
2	12	8.2	105 ± 69	41 ± 16
3	10	6.8	123 ± 67	54 ± 21
4	17	11.6	147 ± 48	73 ± 27
5	13	8.8	148 ± 48	55 ± 14
All	147	100%	177 ± 142	71 ± 31

those of the Hehuang Valley and the eastern Hexi Corridor were above 0.6. Atmospheric aerosols from these areas reached Lanzhou along clusters 1 and 5 and affected the PM<sub>10</sub> concentration. Higher WSCF values of PM<sub>2.5</sub> appeared in the Kumtag Desert, the Qaidam Basin and the Hehuang Valley of Qinghai, Linxia Hui Autonomous Prefecture in Gansu; their potential contribution to PM<sub>2.5</sub> was above 0.4. The PM<sub>2.5</sub> in these areas arrived in Lanzhou along with clusters 1 and 4 (Fig. 8b).

The distribution of the CWT shows the contribution of potential sources to PM<sub>10</sub> and PM<sub>2.5</sub> in Lanzhou (Fig. 9). The Kumtag Desert, Qaidam Basin, and Hehuang Valley, along with the eastern and western Hexi Corridor in Gansu contributed more than 120 µg/m<sup>3</sup> to PM<sub>10</sub> (Fig. 9a), indicating that these regions made the largest contribution the PM<sub>10</sub> concentration in Lanzhou. The Hehuang Valley area and Linxia Hui Autonomous Prefecture contributed more than 60 µg/m<sup>3</sup> to PM<sub>2.5</sub>, indicating that these areas were important sources of PM<sub>2.5</sub> (Fig. 9b).

Discussion

In this study, we found that particulate pollution is extremely severe during the heating season in Lanzhou, Gansu Province, China. Several important factors affect PM concentrations in Lanzhou, including high emissions from local pollution sources (Chu et al., 2008a), special basin topography, poor atmospheric diffusion conditions (Filonchyk & Yan, 2018; Zhang et al., 2001), and dust intrusions from upwind regions (Feng & Wang, 2012). These factors cause the worst air pollution to occur during the heating season.

Meteorological parameters play an important role in regulating PM concentrations (Li et al., 2019; Zhang et al., 2018). Our results demonstrated that daily temperature had a significantly negative effect on the daily PM concentrations. This might be attributable to weaker local diffusion of pollutants and higher pollution emissions in the heating reason (Chu et al., 2008b). Cold surface temperatures in this study led to a stable and shallow surface layer

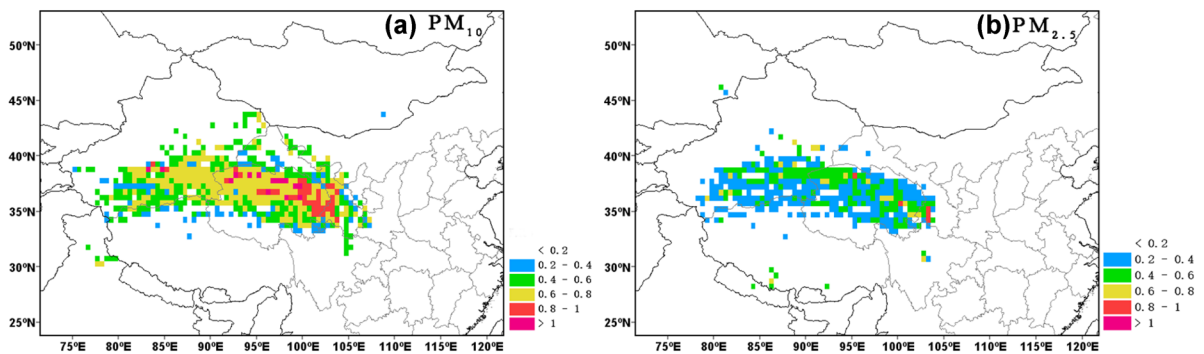


**Fig. 8** The potential source contribution function maps of PM<sub>2.5</sub> and PM<sub>10</sub> in Lanzhou

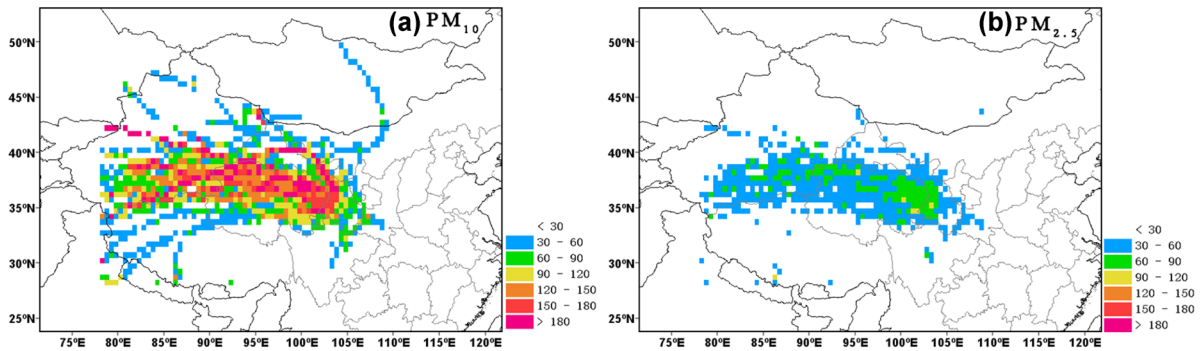


**Fig. 9** The weighted concentration weighted trajectory maps of  $PM_{2.5}$  and  $PM_{10}$  in Lanzhou

caused by strong radiative cooling at night, which suppresses the vertical dispersion of air pollutants (Li et al., 2017). In a similar study, Shakil et al. (2021) found a significant negative correlation between temperature and PM at an urban site in Srinagar, India. A significantly negative relationship was observed between the daily wind speed and the daily  $PM_{2.5}$  and  $PM_{10}$  concentrations. Some previous reports found that strong winds flush out pollutants from the atmosphere and slow winds allow pollution levels to rise (Pateraki et al., 2012; Zhou et al., 2019a). Due to the special basin topography, the daily wind speed in Lanzhou is mostly lower than 3 m/s; this low wind speed will often lead to stable atmospheric conditions and therefore, will limit the dispersion of PM leading to the elevated levels of PM observed in this study. This result agrees with a previous study that was conducted in Lhasa, China (Duo et al., 2018). We found that the  $PBL_{max}$  was also negatively associated with the daily  $PM_{2.5}$  and  $PM_{10}$  concentrations. The boundary layer height usually increases along with solar heating. There is less solar heating in the heating season, which contributed the low  $PBL_{max}$  in the heating season. Thus, a low altitude  $PBL_{max}$  hinders the diffusion of pollutants and create favorable conditions for the accumulation of PM pollutants (Murthy et al., 2020). As a result, the PM concentration gradually increased as the  $PBL_{max}$  decreased in this study. Similar results were also reported in other cities of China, such as Beijing, China and Bet Dagan, Israel (Xiang et al., 2019; Yuval et al., 2020). The relative humidity showed a significantly positive correlation with both  $PM_{10}$  and  $PM_{2.5}$  in this study. Hygroscopic growth is one of the most fundamental properties of atmospheric aerosols. Lou et al. (2017) observed that under

low ( $RH < 70\%$ ) humidity, the accumulation of PM increased significantly. We also discovered that an increase in RH resulted in an increase in the PM concentration due to the hygroscopic growth of particles. This is consistent with consistent with some studies in the Pearl River Delta, China, and in Srinagar, India (Hu et al., 2021; Romshoo et al., 2021).

Previous studies have shown that persistent pollution was not only affected by local emissions and regional transport, but was also restricted by meteorological conditions. The variation of the  $PM_{2.5}$  and  $PM_{10}$  concentrations in the two types of persistent pollution were different (Zhou et al., 2019b). Song et al. (2019) showed the  $PM_{2.5}$  concentration significantly increased during stagnant atmospheric conditions. Jia et al. (2008) studied the variation of atmospheric aerosols in persistent pollution in Beijing, and discovered a growth mechanism characterized by an asymmetric “saw-tooth cycle” including a steady growth baseline in the mechanism, which is mainly based on an increase in secondary inorganic aerosols and an overlap with the daily cycle; this was controlled by the weather cycle. A similar phenomenon was found during Ep2 in this study. The increase in the  $PM_{2.5}/PM_{10}$  ratio over time indicated an increase in fine particulates when the atmosphere was stagnant (low temperature, wind speed, and  $BLH_{max}$  (Fig. 6c, d); this mainly was because the increase in this ratio was promoted by the formation of secondary aerosols from high concentrations of precursors ( $SO_2$ ,  $NO_x$ ) through gas particles (Wu et al., 2019). The study of Yang et al. (2018a) also showed that increased  $PM_{2.5}/PM_{10}$  ratio reflected a rapid secondary formation of particulates in persistent pollution. Because the synoptic circulation was the main factor involved in the



diffusion and accumulation of pollutants, the durations of the sawtooth periods were controlled by synoptic cycles in Ep2. The explosive growth type had also obvious characteristics involving the accumulation of pollutants in stage 1 because of the stagnant atmospheric condition. However, a prominent feature was a sudden increase in  $PM_{10}$  and a sharp decrease in the  $PM_{2.5}/PM_{10}$  ratio in stage 2. Lanzhou is located downwind of some major dust sources in China; this city frequently experiences dust storms in spring and winter. As a result, dust storms have a significant impact on the  $PM_{10}$  concentration (Feng & Wang, 2012). Previous studies in the Hexi Corridor area and the city of Beijing have also reported similar findings (Guan et al., 2017; Tao et al., 2012).

Many studies had pointed out that synoptic circulation and meteorological conditions are the main factors involved in heavy and persistent air pollution (Li et al., 2014; Xu et al., 2020). The typical synoptic conditions that contribute to persistent air pollution in China are weak weather systems, prevailing straight westerly airflow over North China, strong zonal circulation, and weak meridional circulation at 500 hPa (Wang et al., 2014). We also found that the 500 hPa synoptic circulation was mostly controlled by zonal circulation (such as straight westerly airflow and weak frontal systems) of the stagnant type and in stage 1 of the explosive growth type. This was consistent with the results from previous studies (Yang, 2018 b). It is well known that high-pressure systems lead to a widespread downward airflow. At the same time, taking Ep2 as an example, ground meteorological conditions featured low temperatures, wind speeds and  $BLH_{max}$  (Fig. 6c, d). These conditions inhibited the diffusion of air pollutants and enabled pollutants to gradually accumulate; thus, a stable synoptic circulation and adverse meteorological conditions provided a period of continuously stagnant weather with persistent pollution of the stagnant type in this study (Han et al., 2014). Moreover, the backward trajectory analysis showed that the airflow moved across the Huanghuang Valley area of Qinghai (Fig. 5c, d), which was already heavily burdened with  $PM_{2.5}$  pollution. Anthropogenic pollutants from this area aggravated the  $PM_{2.5}$  pollution are presented in Ep2. Dust events in spring and winter are usually associated with frontal and/or cyclonic systems in northern China (Yang et al., 2019b). Lanzhou lays on the southeastern edge of a low-pressure system during

Ep1. Isopiestic were dense and pressure gradients were large, which guided the strong cold air system to Lanzhou. The backward trajectory also indicated that the airflow came from the northwesterly direction of Lanzhou. Moreover, the temperature and RH were remarkably lower than those during the previous stage. This typically indicated the arrival of cold air. A dust storm was also observed at the Zhongchuan Airport Meteorological station. Dust particulates are typically accompanied with the burst of severe cold air mass and lead to an abrupt increase in the  $PM_{10}$  concentration; thus, this was one of the main reasons why the  $PM_{10}$  concentration suddenly increased in the explosive growth type system.

In this study, cluster 1 from the west was the predominant airflow trajectories, followed by cluster 2 from the northwest. This may occur because Lanzhou is located on the northeast edge of the Qinghai-Tibetan Plateau, and the airflow was significantly affected by the topography of this Plateau. A few studies have pointed out the westerly airflow is the main airflow pattern in northwest China because of the obstruction of air masses by the Qinghai-Tibetan Plateau (Guan et al., 2019b; Manabe & Terpstra, 1974). Some studies have pointed out trajectories from various directions had distinct effects on the air quality at the point of reception because of the different pollution emissions in the pathway areas (Liu et al., 2016; Tang et al., 2016). The mean  $PM_{2.5}$  and  $PM_{10}$  concentrations in this study corresponding to various clusters were also significantly different. Clusters 1 and 2 originated from or passed through dust sources including the Kumtag and Qaidam desert as well as the Hexi Corridor. The patterns airflow easily allows air masses to carry large amounts of dust toward Lanzhou when passing through those areas, which gives rise to a significant increase in the  $PM_{10}$  concentration. Luo et al. (2020) reported that dust particles caused significant increases in the  $PM_{10}$  concentration in the area of the present study. Therefore, clusters 1 and 2 were the main transport pathways in Lanzhou for  $PM_{10}$ . Clusters 1 and 2 passed through Hehuang Valley in Qinghai and Linxia Hui Autonomous Region in Gansu, respectively. Air masses in this area were already heavily burdened with  $PM_{2.5}$  pollution in the region surrounding Lanzhou (Fig. 5c, d). The air masses could easily take up anthropogenic pollutants from sources on the ground when passing through this region. Thus, clusters 1 and 2 were the

predominant transport pathway for  $PM_{2.5}$ . Cluster 3 was the northern airflow. The trajectories in cluster 3 may have been associated with deeper Mongolian cyclonic weather systems, resulting in strong wind. These winds facilitated the ventilation and vertical mixing of pollutants while bringing in fresh air from sparsely populated and less industrialized northern regions such as the Ningxia Hui Autonomous Region and north-central Gansu. Thus, the airflow trajectories associated with cluster 2 had less impact on  $PM_{10}$  and  $PM_{2.5}$  loadings in Lanzhou.

$PM_{10}$  is emitted from natural sources such as dust storms, sea salt, volcanic eruptions, and biological particles (Guan et al., 2019a). The strongest potential sources of  $PM_{10}$  in this study were mainly located in the Kumtag Desert, the Qaidam Basin, and the western Hexi Corridor (Figs. 8a and 9a). These areas have arid climates, experience strong winds, and have aeolian land with low vegetation cover that are conducive to the formation of dust storms, making them important dust sources in China (Qian et al., 2004; Song et al., 2016). Lanzhou is located downwind from these areas (Fig. 1), so that the airflow passing through these areas easily picks up large amounts of dust particulates and carries them toward Lanzhou, which gives rise to significant increase in  $PM_{10}$  concentration. The results indicated that these regions were important potential source areas of  $PM_{10}$  in Lanzhou. Some studies have also found that these areas are important potential sources of  $PM_{10}$  for many cities in northwest China (Guan et al., 2019a; Yang et al., 2019a). Some scholars have pointed out that areas with limited plant cover including croplands, grasslands, and cropland mosaics are the main sources of anthropogenic dust (Guan et al., 2015; Chen et al., 2018). The present study found that the eastern part of the Hexi Corridor was also an important potential source area for  $PM_{10}$ . This mainly occurs because that the region is an important agricultural area in northwest China (Figs. 8a and 9a). In winter and spring, when the farmland lays fallow or some crops are in the seedling stage, the ability of soil particles to consolidate is weak (Yan et al., 2009), and frequent windy weather and increased human activity can easily release dust particulates into the upper air stream (Goudie & Middleton, 2001; Hooper & Marx, 2018), resulting in the region becoming major potential sources of  $PM_{10}$  for Lanzhou (Yan et al., 2009). The  $PM_{2.5}$  pollution is mainly derived from anthropogenic emission sources including transportation, fuel burning, and industrial processes

(Jain et al., 2020). Previous studies have reported the high PSCF and CWT values coincided with the locations of densely populated and industrial areas (Jeong et al., 2017; Saxena et al., 2017). The Hehuang Valley and Linxia Hui Autonomous Region are densely populated and economically developed areas with the areas surrounding Lanzhou (Wang, 2013). Frequent human activities usually release abundant particulate pollutants and their precursors, which causes serious  $PM_{2.5}$  pollution. According to the Environmental Bulletin of Qinghai Province in 2017, the mean annual concentrations of  $PM_{2.5}$  in the cities of Xining and Haidong, two important cities located in Hehuang valley, were  $39 \mu\text{g m}^{-3}$  and  $47 \mu\text{g m}^{-3}$ , respectively, which exceeded the Chinese Ambient Air Quality Grade II annual standard ( $35 \mu\text{g m}^{-3}$ ). As a result, these make a strong contribution to  $PM_{2.5}$ .

## Conclusion

This paper analyzed the formation mechanism of persistent pollution, qualitatively identified major pollution transport pathways and potential source regions, and quantified the regionally transported contributions to  $PM_{2.5}$  and  $PM_{10}$  loadings in Lanzhou during the heating season from November 2016 to March 2017.

During the entire period, the daily mean concentrations of  $PM_{10}$  and  $PM_{2.5}$  reached  $177 \pm 142 \text{ g/m}^3$  and  $70 \pm 32 \mu\text{g/m}^3$ , respectively; the days over the Grade II standard accounted for 53% and 36% of all days, respectively, and particulate pollution was serious.

Five episodes with persistent air pollution were observed, which were classified into either the stagnant accumulation or explosive growth type based on the mechanism of pollution formation and evolution. Under the influence of stagnant weather, the concentration of  $PM_{2.5}$  and  $PM_{10}$  and  $PM_{2.5}/PM_{10}$  ratio followed a growing “saw-tooth cycle” pattern during stagnant accumulation episodes. Dust storms created a prominent feature in which  $PM_{10}$  increased suddenly and the  $PM_{2.5}/PM_{10}$  ratio decreased sharply in explosive growth type episodes.

Trajectories were grouped into five clusters. Cluster 1 came from the west and had the highest frequency (64.6%) of all of episode clusters, followed by cluster 4 from the northwest with 11.6%. Cluster 4 contributed the least (4.6%) to the total trajectories.

The highest PM<sub>10</sub> concentrations were observed in clusters 1 and 5 at 205 ± 176 µg/m<sup>3</sup> and 148 ± 48 µg/m<sup>3</sup>, respectively. The highest PM<sub>2.5</sub> concentrations were observed in clusters 1 and 4 at 78 ± 33 µg/m<sup>3</sup> and 73 ± 27 µg/m<sup>3</sup>, respectively. The lowest PM<sub>10</sub> and PM<sub>2.5</sub> concentrations were found in cluster 2 at 105 ± 27 µg/m<sup>3</sup> and 41 ± 33 µg/m<sup>3</sup>, respectively.

The potential sources of PM<sub>10</sub> were mainly distributed in the Kumtag Desert in Xinjiang, the Qaidam Basin and Hehuang Valley in Qinghai, and the western and eastern Hexi Corridor in Gansu, where the contributions to PM<sub>10</sub> were more than 120 µg/m<sup>3</sup>. The important potential sources of PM<sub>2.5</sub> in Lanzhou were located in Hehuang Valley in Qinghai and Linxia Hui Autonomous Prefecture in Gansu; the contributions to PM<sub>2.5</sub> from these areas were more than 60 µg/m<sup>3</sup>.

**Author contribution** Yongtao Guo and Dandan Li: conceptualization, methodology, writing; Yuxia Ma and Qidong Yang: reviewing; Jiangping Li: data curation; Lingbo Wei: software; Chunying Lin: analysis; Hang Wang and JiahuiShen: original draft preparation.

**Funding** This research is supported by the National Natural Science Foundation of China (Grant No. 41975141) and the Qinghai Science and Technology Department (Grant No. 2017-ZJ-799).

**Data availability** Data will be available on request.

**Declarations**

**Ethics approval** This article does not contain any studies with human participants or animals performed by any of the authors.

**Consent to participate** Not applicable.

**Consent to publish** Not applicable.

**Conflict of interest** The authors declare no conflict of interest.

**References**

An, X. Q., Zuo, H. C., & Chen, L. J. (2007). Atmospheric Environmental Capacity of SO<sub>2</sub> in Winter over Lanzhou in China: A Case Study. *Advances in Atmospheric Sciences*, 24, 688–699.

Annalis, D. B., Anna, M. I., Stefano, C., Cinzia, P., Francesca, B., Luca, T., Monica, C., Luca, D. L., Gabriele, M., Anna M. S., & Marco, C. (2021). Impact of synoptic meteorological

conditions on air quality in three different case studies in Rome, Italy. *Atmospheric Pollution Research*, 12, 76–88. <https://doi.org/10.1016/j.apr.2021.02.019>

Bi, S. J., Yang, L. X., Zhang, Y., Huang, Q., Li, J. S., Zhao, T., Zhang, X. F., Wang, P. C., & Wang, W. X. (2021). Source appointment of PM<sub>2.5</sub> in Qingdao Port, East of China. *Science of the Total Environment*, 755, 1424–56. <https://doi.org/10.1016/j.scitotenv.2020.142456>

Chen, S. Y., Jiang, N. X., Huang, J. P., Xu, X. G., Zhang, H. W., Zhou, Z. G., Huang, K. G., Xu, X. C., Wei, Y., Guan, X. D., Zhang, X. R., Luo, Y., Hu, Z. Y., & Feng, T. C. (2018). Quantifying contributions of natural and anthropogenic dust emission from different climatic regions. *Atmospheric Environment*, 191, 94–104. <https://doi.org/10.1016/j.atmosenv.2018.07.043>

Chen, T., Deng, S. L., Gao, Y., Qu, L., Li, M. C., & Chen, D. (2017). Characterization of air pollution in urban areas of Yangtze River delta, China. *Chinese Geographical Science*, 27, 836–846.

Cheng, B. W., Ma, Y. X., Feng F. L., Zhang, Y. F., Shen, J. H., Wang, H., Guo, Y. T., & Cheng Y. F. (2021). Influence of weather and air pollution on concentration change of PM<sub>2.5</sub> using a generalized additive model and gradient boosting machine. *Atmospheric Environment*, 255(15), 118437. <https://doi.org/10.1016/j.atmosenv.2021.118437>

Chifflet, S., Amouroux, D., Bérail, S., Barre, J., Van, T. C., Baltrons, O., Brune, J., Dufour, A., Guino, B., & Mari, X. (2018). Origins and discrimination between local and regional atmospheric pollution in Haiphong (Vietnam), based on metal(loid) concentrations and lead isotopic ratios in PM<sub>10</sub>. *Environmental Science and Pollution Research*, 25, 26653–26668.

Chu, P. C., Chen, Y. H., Lu, S. H., Li, Z. C., & Lu, Y. Q. (2008a). Particulate air pollution in Lanzhou China. *Environment International*, 34, 698–713.

Chu, P. C., Chen, Y. H., & Lu, S. H. (2008b). Afforestation for reduction of NO<sub>x</sub> concentration in Lanzhou China. *Environment International*, 34, 688–697. <https://doi.org/10.1016/j.envint.200712.014>

Deng, X. L., Cao, W. H., Huo, Y. F., Yang, G. Y., Yu, C. X., He, D. Y., Deng, W. T., Fu, W., Ding, H. M., Zhai, J., Cheng, L., & Zhao, X. H. (2019). Meteorological conditions during a severe, prolonged regional heavy air pollution episode in eastern China from December 2016 to January 2017. *Theoretical and Applied Climatology*, 135, 1105–1122.

Duo, B., Cui, L. L., Wang, Z. Z., Li, R., Zhang, L. W., Fu, H. B., Chen, J. M., Zhang, H. F., & Zhang, A. Q. (2018). Observations of atmospheric pollutants at Lhasa during 2014–2015: Pollution status and the influence of meteorological factors. *Journal of Environmental Sciences*, 63, 28–42. <https://doi.org/10.1016/j.jes.2017.03.010>

Draxler, R. R., & Hess, G. D. (1998). An overview of the HYSPLIT 4 modeling system for trajectories, dispersion, and deposition. *Australian Meteorological Magazine*, 47, 295–308.

Dimitriou, K., & Kassomenos, P. (2018). A meteorological analysis of PM<sub>10</sub> episodes at a high altitude city and a low altitude city in central Greece—The impact of wood burning heating devices. *Atmospheric Research*, 214(1), 329–337. <https://doi.org/10.1016/j.atmosres.2018.08.014>

- Feng, X. Y., & Wang, S. G. (2012). Influence of different weather events on concentrations of particulate matter with different sizes in Lanzhou. *China Journal of Environmental Sciences*, 24(4), 665–667. [https://doi.org/10.1016/S1001-0742\(11\)60807-3](https://doi.org/10.1016/S1001-0742(11)60807-3)
- Filonchik, M., & Yan, H. (2018). The characteristics of air pollutants during different seasons in the urban area of Lanzhou. *Northwest China Environmental Earth Sciences*, 77(22), 1–17.
- Gowan, M., & Andrew, C. (2008). Identification of dust transport pathways from Lake Eyre, Australia using Hysplit Hamish. *Atmospheric Environment*, 42(29), 6915–6925. <https://doi.org/10.1016/j.atmosenv.2008.05.053>
- Goudie, A. S., & Middleton, N. J. (2001). Saharan dust storms: nature and consequences. *Earth-Science Reviews*, 56(1–4), 179–204. [https://doi.org/10.1016/S0012-8252\(01\)00067-8](https://doi.org/10.1016/S0012-8252(01)00067-8)
- Guan, Q. Y., Cai, A., Wang, F. F., Yang, L. Q., Xu, C. Q., & Liu, Z. Y. (2017). Spatio-temporal variability of particulate matter in the key part of Gansu Province, Western China. *Environmental Pollution*, 230, 189–198. <https://doi.org/10.1016/j.envpol.2017.06.045>
- Guan, Q. Y., Li, F. C., Yang, L. Q., Zhao, R., Yang, Y. Y., & Luo, H. P. (2018). Spatial-temporal variations and mineral dust fractions in particulate matter mass concentrations in an urban area of northwestern China. *Journal of Environmental Management*, 222, 95–103. <https://doi.org/10.1016/j.jenvman.2018.05.064>
- Guan, Q. Y., Luo, H. P., Pan, N. H., Zhao, R., Yang, L. Q., Yang, Y. Y., & Tian, J. (2019a). Contribution of dust in northern China to PM<sub>10</sub> concentrations over the Hexi corridor. *Science of The Total Environment*, 660, 947–958. <https://doi.org/10.1016/j.scitotenv.2018.12.412>
- Guan, Q. Y., Yang, Y. Y., Luo, H. P., Zhao, R., Pan, N. H., Lin, J. K., & Yang, L. Q. (2019b). Transport pathways of PM<sub>10</sub> during the spring in northwest China and its characteristics of potential dust sources. *Journal of Cleaner Production*, 237, 117746. <https://doi.org/10.1016/j.jclepro.2019.117746>
- Guan, X., Huang, J., Zhang, Y., Xie, Y. K., & Liu, J. J. (2015). The relationship between anthropogenic dust and population over global semi-arid regions. *Atmospheric Chemistry and Physics*, 16(5159–5169), 2016. <https://doi.org/10.5194/acp-16-5159-2016>
- Han, S. Q., Wu, J. H., Zhang, Y. F., Cai, Z. Y., Feng, Y. C., Yao, Q., Li, X. J., Liu, Y. W., & Zhang, M. (2014). Characteristics and formation mechanism of a winter haze–fog episode in Tianjin, China. *Atmospheric Environment*, 98, 323–330. <https://doi.org/10.1016/j.atmosenv.2014.08.078>
- Holzworth, G. C. (1964). Estimates of mean maximum mixing depths in the contiguous United States. *Monthly Weather Review*, 92(5), 235–242.
- Hooper, J., & Marx, S. (2018). A global doubling of dust emissions during the Anthropocene. *Global and Planetary Change*, 169, 70–91. <https://doi.org/10.1016/j.gloplacha.2018.07.003>
- Hong, Q. Q., Xie, Z. Q., Liu, C., Wang, F. Y., Xie, P. H., Kang, H., Xu, J., Wang, J. C., Wu, F. C., He, P. Z., Mou, F. S., Fan, S. D., Dong, Y. S., Zhan, H. C., Yu, X. W., Chi, X. Y., Liu, J. G. (2016) Speciated atmospheric mercury on haze and non-haze days in an inland city in China. *Atmospheric Chemistry and Physics*, 16, 13807–13821 <https://doi.org/10.5194/acp-16-13807-2016>
- Hsu, Y. K., Holsen, T. M., & Hopke, P. K. (2003). Comparison of hybrid receptor models to locate PCB sources in Chicago. *Atmospheric Environment*, 37, 545–562. [https://doi.org/10.1016/S1352-2310\(02\)00886-5](https://doi.org/10.1016/S1352-2310(02)00886-5)
- Hu, M. M., Wang, Y. F., Wang, S., Jiao, M. Y., Huang, G. H., & Xia, B. C. (2021). Spatial-temporal heterogeneity of air pollution and its relationship with meteorological factors in the Pearl River Delta. *China Atmospheric Environment*, 254, 118415. <https://doi.org/10.1016/j.atmosenv.2021.118415>
- Huang, F., Zhou, J. B., Chen, N., Li, Y., Li, K., & Wu, S. P. (2019). Chemical characteristics and source apportionment of PM<sub>2.5</sub> in Wuhan. *China Journal of Atmospheric Chemistry*, 76, 245–262.
- Jain, S., Sharma, S. K., Vijayan, N., & Mandal, T. K. (2020). Seasonal characteristics of aerosols (PM<sub>2.5</sub> and PM<sub>10</sub>) and their source apportionment using PMF: A four year study over Delhi, India. *Environmental Pollution*, 262, 114337. <https://doi.org/10.1016/j.envpol.2020.114337>
- Jeong, J. H., Shon, Z. H., Kang, M., Song, S. K., Kim, Y. K., Park, J., & Kim, H. (2017). Comparison of source apportionment of PM<sub>2.5</sub> using receptor models in the main hub port city of East Asia: Busan. *Atmospheric Environment*, 148, 115–127. <https://doi.org/10.1016/j.atmosenv.2016.10.055>
- Jia, Y., Rahn, K. A., He, K., Wen, T. X., & Wang, Y. S. (2008). A novel technique for quantifying the regional component of urban aerosol solely from its sawtooth cycles. *Journal of Geophysical Research: Atmospheres*, 11(D21), 6089–6098. <https://doi.org/10.1029/2008JD>
- Kozáková, J., Pokorná, P., Vodička, P., Lucie, O., Jakub, O., Křůmal, K., Mikuška, P., Hovorka, J., Moravec, P., & Schwarz, J. (2019). The influence of local emissions and regional air pollution transport on a European air pollution hot spot. *Environmental Science and Pollution Research*, 26, 1675–1692.
- Li, R., Wang, Z. Z., Cui, L. L., Fu, H. B., Zhang, L. W., Kong, L. D., Chen, W. D., & Chen, J. M. (2019). Air pollution characteristics in China during 2015–2016: Spatiotemporal variations and key meteorological factors. *Science of The Total Environment*, 648, 902–915. <https://doi.org/10.1016/j.scitotenv.2018.08.181>
- Li, L., Qian, J., Ou, C. Q., Zhou, Y. X., Guo, C., & Guo, Y. M. (2014). Spatial and temporal analysis of Air Pollution Index and its timescale-dependent relationship with meteorological factors in Guangzhou, China, 2001–2011. *Environmental Pollution*, 190, 75–81. <https://doi.org/10.1016/j.envpol.2014.03.020>
- Li, L., Yan, D., Xu, S., Huang, M., Wang, X., & Xie, S. D. (2017). Characteristics and source distribution of air pollution in winter in Qingdao, eastern China. *Environmental Pollution*, 224, 44–53. <https://doi.org/10.1016/j.envpol.2016.12.037>
- Li, X. C. (2018). Study on the classification of polluted weather during the heating period in Lanzhou (PP22). Lanzhou University, Dissertation
- Liu, B. S., Liang, D. N., Yang, J. M., Dai, Q. L., & Bi, X. H. (2016). Characterization and source apportionment of volatile organic compounds based on 1-year of observational data in Tianjin, China. *Environmental Pollution*, 218, 757–769. <https://doi.org/10.1016/j.envpol.2016.07.072>



Liu, Q., Cheng, N. X., He, Q. S., Chen, Y. H., Liu, T. Q., Liu, X., Zhang, H., Li, J. Z., Zhan, Q. Y. (2020) Meteorological conditions and their effects on the relationship between aerosol optical depth and macro-physical properties of warm clouds over Shanghai based on MODIS. *Atmospheric Pollution Research*, 1637–1644. <https://doi.org/10.1016/j.apr.2020.07.001>

Liu, X. G., Li, J., Qu, Y., Han, T., Hou, L., Gu, C., Chen, Y., Yang, X., Liu, T., Yang, Y., Zhang, H., & Hu, M. (2013). Formation and evolution mechanism of regional haze: A case study in the megacity Beijing, China. *Atmospheric Chemistry and Physics*, 13, 4501–4514. <https://doi.org/10.5194/acp-13-4501-2013>

Liu, Y. C., Zhao, H. J., Ma, Y. J., Yang, H. B., Wang, Y. F., Wang, H. Y., Zhang, Y. H., Zou, X. D., Wang, H. B., Wen, R. H., Zhao, Z. Q., & Quan, W. J. (2021). Characteristics of particulate matter and meteorological conditions of a typical air-pollution episode in Shenyang, northeastern China, in winter 2017. *Atmospheric Pollution Research*, 12, 316–327. <https://doi.org/10.1016/j.apr.2020.09.007>

Lou, C., Liu, H., Li, Y., Peng, Y., Wang, J., & Dai, L. (2017). Relationships of relative humidity with PM<sub>2.5</sub> and PM<sub>10</sub> in the Yangtze River Delta. *China. Environmental Monitoring and Assessment*, 189, 1–16.

Luo, H. P., Guan, Q. Y., Pan, N. H., Wang, Q. Z., Li, H., Li, H. C., Lin, J. K., Tan, Z., & Shao, W. Y. (2020). Using composite fingerprints to quantify the potential dust source contributions in northwest China. *Science of The Total Environment*, 742, 140560. <https://doi.org/10.1016/j.scitotenv.2020.140560>

Ma, Y. X., Zhang, H. P., Zhao, Y. X., Zhou, J. D., Yang, S. X., Zheng, X. D., & Wang, S. G. (2017). Short-term effects of air pollution on daily hospital admissions for cardiovascular diseases in western China. *Environmental Science and Pollution Research*, 24, 14071–14079.

Manabe, S., & Terpstra, T. B. (1974). The effects of mountains on the general circulation of the atmosphere as identified by numerical experiments. *Journal of the Atmospheric Sciences*, 31(1), 3–42. <https://doi.org/10.1016/j.jastp.2019.105157>

Murthy, B. S., Latha, R., Tiwari, A. P., Rathod, A. D., Singh, S. (2020). G. Beig Impact of mixing layer height on air quality in winter. *Journal of Atmospheric and Solar-Terrestrial Physics*, 197, 105157.

Pateraki, S., Asimakopoulos, D. N., Flocas, H. A., Maggos, T., & Vasilakos, C. (2012). The role of meteorology on different sized aerosol fractions (PM<sub>10</sub>, PM<sub>2.5</sub>, PM<sub>2.5-10</sub>). *Science of The Total Environment*, 419(1), 124–135. <https://doi.org/10.1016/j.scitotenv.2011.12.064>

Qian, W. H., Tang, X., & Quan, L. S. (2004). Regional characteristics of dust storms in China. *Atmospheric Environment*, 38, 4895–4907. <https://doi.org/10.1016/j.atmosenv.2004.05.038>

Romshoo, S. A., Bhat, M. A., Romshoo, G. B., Bhat, M. A., & Gufran, B. (2021). Particulate pollution over an urban Himalayan site: Temporal variability, impact of meteorology and potential source regions. *Science of the Total Environment*, 799, 149364. <https://doi.org/10.1016/j.scitotenv.2021.149364>

Saxena, M., Sharma, A., Sen, A., Saxena, P., Mandal, T. K., Sharma, S. K., & Sharma, C. (2017). Water soluble inorganic species of PM<sub>10</sub> and PM<sub>2.5</sub> at an urban site of Delhi, India: Seasonal variability and sources. *Atmospheric Research*, 184, 112–125. <https://doi.org/10.1016/j.atmosres.2016.10.005>

Sirois, A., & Bottenheim, J. W. (1995). Use of backward trajectories to interpret the 5-year record of PAN and O<sub>3</sub> ambient air concentrations at Kejimikujik National Park, Nova Scotia. *Journal of Geophysical Research: Atmospheres*, 100(D2), 2867–2881. <https://doi.org/10.1029/94JD02951>

Shakil, A. R., Bhat, M. A., & Beig, G. (2021). Particulate pollution over an urban Himalayan site: Temporal variability, impact of meteorology and potential source regions. *Science of the Total Environment*, 799, 149364. <https://doi.org/10.1016/j.scitotenv.2021.149364>

Shi, Y., Hu, F., Xiao, Z. S., Fan, G. Q., & Zhang, Z. (2020). Comparison of four different types of planetary boundary layer heights during a haze episode in Beijing. *Science of the Total Environment*, 711, 134928. <https://doi.org/10.1016/j.scitotenv.2019.134928>

Song, M. D., Liu, X. G., Tan, Q. W., Feng, M., Qu, Y., An, J. L., & Zhang, Y. H. (2019). Characteristics and formation mechanism of persistent extreme haze pollution events in Chengdu, southwestern China. *Environmental Pollution*, 251, 1–12. <https://doi.org/10.1016/j.envpol.2019.04.081>

Song, H. Q., Zhang, K. H., Piao, S. L., & Wan, S. Q. (2016). Spatial and temporal variations of spring dust emissions in northern China over the last 30 years. *Atmospheric Environment*, 126, 117–127. <https://doi.org/10.1016/j.atmosenv.2015.11.052>

Sun, J., Gong, J. H., Zhou, J. P., Liu, J. T., & Liang, J. M. (2019). Analysis of PM<sub>2.5</sub> pollution episodes in Beijing from 2014 to 2017: Classification, interannual variations and associations with meteorological features. *Atmospheric Environment*, 213, 384–394. <https://doi.org/10.1016/j.atmosenv.2019.06.015>

Tan, T. Y., Hu, M., Li, M. R., Guo, Q. F., Wu, Y. S., Fang, X., Gu, F. T., Wang, Y., & Wu, Z. J. (2018). New insight into PM<sub>2.5</sub> pollution patterns in Beijing based on one-year measurement of chemical compositions. *Science of the Total Environment*, 621,734–743. <https://doi.org/10.1016/j.scitotenv.2017.11.208>

Tang, L. L., Yu, H. G., Ding, A. J., Zhang, Y. J., Qin, W., Wang, Z., Chen, W. T., Hua, Y., & Yang X. X. (2016). Regional contribution to PM<sub>1</sub> pollution during winter haze in Yangtze River Delta, China. *Science of The Total Environment*, 541, 161–166. <https://doi.org/10.1016/j.scitotenv.2015.05.058>

Tao, M. H., Chen, L. G., Su, L., & Tao, J. H. (2012). Satellite observation of regional haze pollution over the North China Plain. *Journal of Geophysical Research: Atmospheres*, 117, D12203. <https://doi.org/10.1029/2012JD017915>

Wang, L. L., Liu, Z. R., Sun, Y., Ji, D. S., & Wang, Y. S. (2015). Long-range transport and regional sources of PM<sub>2.5</sub> in Beijing based on long-term observations from 2005 to 2010. *Atmospheric Research*, 157,37–483. <https://doi.org/10.1016/j.atmosres.2014.12.003>

Wang, S.G., Jiang, D. B., Yang, D. B., Shang, K. Z., & Bin. Q. (2000). A Study on characteristics of change of maximum mixing depths in Lanzhou. *Plateau Meteorology*, 19(3), 363–370.

- Wang, Y. Q., Zhang, X. Y., & Draxler, R. R. (2009). TrajStat: GIS-based software that uses various trajectory statistical analysis methods to identify potential sources from long-term air pollution measurement data. *Environmental Modelling and Software*, 24, 938–939.
- Wang, Y. S., Yao, L., Wang, L. L., Liu, Z. R., Ji, D. S., Tang, G. Q., Zhang, J. K., Sun, Y., Hu, B., & Xin, J. Y. (2014). Mechanism for the formation of the January 2013 heavy haze pollution episode over central and eastern China. *Science China: Earth Sciences*, 57(1), 14–25.
- Wang, Z. H. (2013). Research on co-ordinate the urban and rural industrial Development in Hehuang Valley of Qinghai Province (pp20–22). Qinghai Normal University, Dissertation.
- Wu, X., Xu L. L., Hong, Y. W., Chen, J. F., Qiu, Y. Q., Hu, B. Y., Hong, Z. Y., Zhang, Y. R., Liu, T. T., Chen, Y. T., Bian, Y. H., Zhao, G. Q., Chen, J. S., & Li, M. R. (2019). The air pollution governed by subtropical high in a coastal city in Southeast China: Formation processes and influencing mechanisms. *Science of The Total Environment*, 692, 1135–1145. <https://doi.org/10.1016/j.scitotenv.2019.07.341>
- Xiang, Y., Zhang, T. S., Liu, J.G., Lv, L. H., Dong, Y. S., & Chen, Z. Y. (2019). Atmosphere boundary layer height and its effect on air pollutants in Beijing during winter heavy pollution. *Atmospheric Research*, 215(1), 305–316. <https://doi.org/10.1016/j.atmosres.2018.09.014>
- Xu, Y. L., Xue, W. B., Yu, L., Huang, Q., Zhao, Y., Cheng, S. Y., Ren, Z. H., & Wang, J. N. (2020). Spatiotemporal variation in the impact of meteorological conditions on PM<sub>2.5</sub> pollution in China from 2000 to 2017. *Atmospheric Environment*, 223, 117215. <https://doi.org/10.1016/j.atmosenv.2019.117215>
- Yan, C. Z., Zhou, Y. M., Song, X., & Duan, H. C. (2009). Estimation of areas of sand and dust emission in the Hexi Corridor from a land cover database: An approach that combines remote sensing with GIS. *Environmental Geology*, 57, 707–713.
- Yang, J. H., Ji, Z. M., Kang, S. C., Zhang, Q. G., Chen, X. T., & Lee, S. Y. (2019a). Spatiotemporal variations of air pollutants in western China and their relationship to meteorological factors and emission sources. *Environmental Pollution*, 254, 112952. <https://doi.org/10.1016/j.envpol.2019.112952>
- Yang, M. Z., Zhu, X. Y., Pan, H. G., Ai, W. X., Song, W. L., & Pan, Y. P. (2019b). Changes of the relationship between spring sand dust frequency and large scale atmospheric circulation. *Atmospheric Research*, 125, 188–198. <https://doi.org/10.1016/j.atmosres.2019.04.004>
- Yang, S., Ma, Y. L., Duan, F. K., He, K. B., Wang, L. T., Wei, Z., Zhu, L. D., Ma, T., Li, H., & Ye, S. Q. (2018). Characteristics and formation of typical winter haze in Handan, one of the most polluted cities in China. *Science of the Total Environment*, 613–614, 1367–2137. <https://doi.org/10.1016/j.scitotenv.2017.08.033>
- Yang, X. L. (2018b). The synoptic type and meteorological condition during extreme air pollution events in Lanzhou city. Dissertation University of Lanzhou.
- Yang, Y. R., Liu, X. G., Qu, Y., Wang, J. L., An, J. L., Zhang, Y. H., & Zhang F. (2015). Formation mechanism of continuous extreme haze episodes in the megacity Beijing, China, in January 2013. *Atmospheric Research*, 155, 192–203. <https://doi.org/10.1016/j.atmosres.2014.11.023>
- Yu, H., Feng, J. L., & Su, X. F. (2020). A seriously air pollution area affected by anthropogenic in the central China: Temporal–spatial distribution and potential sources. *Environmental Geochemistry and Health*, 42, 3199–3211.
- Yuval, Y. L., Uri, D. Y., Ilan, L., & David, M. B. (2020). On the association between characteristics of the atmospheric boundary layer and air pollution concentrations. *Atmospheric Research*, 231, 104675. <https://doi.org/10.1016/j.atmosres.2019.104675>
- Zhao, M. F., Qiao, T., Li, Y. L., Tang, X. X., Xiu, G. L., & Yu, J. Z. (2016). Temporal variations and source apportionment of Hulis-C in PM<sub>2.5</sub> in urban Shanghai. *Science of the Total Environment*, 571, 18–26. <https://doi.org/10.1016/j.scitotenv.2016.07.127>
- Zhang, L., Chen, C. H., & Murlis, J. (2001). Study on winter air pollution control in Lanzhou, China. *Water, Air, and Soil Pollution*, 127, 351–372.
- Zhang, L., Wang, S. X., Wang, L., & Hao, J. M. (2013). Atmospheric mercury concentration and chemical speciation at a rural site in Beijing, China: Implications of mercury emission sources. *Atmospheric Chemistry and Physics*, 13, 10505–10516. <https://doi.org/10.5194/acp-13-10505-2013>.
- Zhang, Q., & Hu, Y. (1998). Shallow discussion on some problems of pollution and its controlling of atmospheric environment over the Lanzhou City. *Plateau Meteorology*, 17(2), 202–210.
- Zhang, Q., & Li, H. Y. (2011). A Study of the relationship between air pollutants and inversion in the ABL over the city of Lanzhou. *Advances in Atmospheric Sciences*, 28, 879–886.
- Zhang, Q. Q., Ma, Q., Zhao, B., Liu, X. Y., Wang, Y. X., Jia, B. X., & Zhang, X. Y. (2018). Winter haze over North China Plain from 2009 to 2016: Influence of emission and meteorology. *Environmental Pollution*, 242, 1308–1318. <https://doi.org/10.1016/j.envpol.2018.08.019>
- Zhou, Y., Bai, Y. Q., Yue, Y. Y., Lü, J. J., Chen, S. N., & Xiao, H. (2019a). Characteristics of the factors influencing transportation and accumulation processes during a persistent pollution event in the middle reaches of the Yangtze River, China. *Atmospheric Pollution Research*, 10, 1420–1434. <https://doi.org/10.1016/j.apr.2019.03.014>
- Zhou, Y., Luo, B., Li, J., Yue, Y. Y., Lü, J. J., Chen, S. N., & Xiao, H. (2019b). Characteristics of six criteria air pollutants before, during, and after a severe air pollution episode caused by biomass burning in the southern Sichuan Basin, China. *Atmospheric Environment*, 215, 116840. <https://doi.org/10.1016/j.apr.2019.03.014>
- Zhu, J., Zhu, B., Huang, Y., An, J. L., Xu, J. P. (2019) PM<sub>2.5</sub> vertical variation during a fog episode in a rural area of the Yangtze River Delta China. *Science of the Total Environment*, 685, 555–563. <https://doi.org/10.1016/j.scitotenv.2019.05.319>

**Publisher's Note** Springer Nature remains neutral with regard to jurisdictional claims in published maps and institutional affiliations.